

# Symbol-Aware Precoder Design for Physical-Layer Anonymous Communications

Yu Li, Milad Tatar Mamaghani, Xiangyun Zhou, *Fellow, IEEE*, and Nan Yang, *Senior Member, IEEE*

**Abstract**—Physical-layer characteristics, such as channel state information (CSI) and transmitter noise induced by hardware impairments, are often uniquely associated with a transmitter. This paper investigates transmitter anonymity at the physical layer from a signal design perspective. We consider an anonymous communication problem where the receiver should reliably decode the signal from the transmitter but should not make use of the signal to infer the transmitter’s identity. Transmitter anonymity is quantified using a Kullback-Leibler divergence (KLD)-based metric, which enables the formulation of explicit anonymity constraints in the precoder design. We then propose an anonymous symbol-level precoding strategy that preserves reliable communication under spatial multiplexing while preventing transmitter identification. The proposed framework employs a partitioned equal-gain combining (P-EGC) scheme that leverages receiver diversity without requiring transmitter-specific CSI. Simulation results demonstrate anonymity-reliability tradeoffs across different signal-to-noise ratios (SNRs) and numbers of data streams. Moreover, the results reveal opposite trends of anonymity with respect to transmitter-dependent noise variations in the low-SNR and high-SNR regimes.

**Index Terms**—Physical-layer anonymous communications, symbol-level precoding, MIMO, Kullback-Leibler divergence

## I. INTRODUCTION

THE proliferation of next-generation wireless networks is reshaping the landscape of communications by enabling a broad spectrum of Internet of Things (IoT) applications, including vehicular networks, uncrewed aerial vehicle (UAV) communications, and body sensor systems [1]–[3]. While these advances offer unprecedented connectivity, the broadcast nature of wireless transmissions inherently exposes such systems to various security threats such as eavesdropping, jamming, spoofing, and traffic analysis [4]–[6]. These vulnerabilities are particularly critical in human-centric IoT services, where sensitive information, such as user identities, locations, and physiological data, is routinely exchanged, and unauthorized disclosure may lead to severe privacy violations and safety risks [7], [8].

Conventional upper-layer security mechanisms often face practical limitations in IoT environments, due to stringent constraints on power consumption, computational capability, and latency [9]. In this context, physical-layer security (PLS) has emerged as an effective security enhancement by exploiting the intrinsic properties of wireless channels and transmit

signals to provide lightweight and scalable protection, without relying on computationally intensive and complex cryptographic protocols. Under the general umbrella of PLS, two complementary objectives can be identified: *confidentiality*, which safeguards the transmitted content from unauthorized access [10]–[12], and *privacy*, which prevents adversaries—or even legitimate parties—from inferring sensitive user-related information, such as the identity or even the existence of the transmitter, from the received signals. Privacy-oriented techniques are generally developed under two different principles: anonymity aims to conceal the transmitter’s identity within a group of potential users [13], whereas unobservability seeks to hide the very existence of transmissions, often through low-intercept-probability communications such as covert communications [14].

Transmitter anonymity is particularly critical in several emerging wireless applications. In vehicular systems, periodic beaconing enables safety-critical functions, such as navigation and collision avoidance, yet roadside adversaries can exploit physical-layer signal characteristics to perform persistent vehicle identification and trajectory reconstruction, even in the presence of pseudonym-based protocols [15], [16]. Similar vulnerabilities arise in UAV communications, where transmitter identification can expose mission-critical information and enable tracking, jamming, or physical capture [17]–[19]. In body area networks, physical-layer identification by third-party base stations can further link sensitive physiological data to individual users, leading to severe privacy violations and potential commercial exploitation [20]. In these scenarios, the physical-layer signals often carry device-specific information or location-dependent channel characteristics, which can be exploited for transmitter identification. Therefore, anonymity mechanisms operating above the physical layer may no longer be sufficient against adversaries capable of exploiting physical-layer features. This limitation motivates the development of physical-layer anonymity techniques that aim to mitigate identity leakage at the signal level [21].

### A. Related Works

In this work, we focus on the analysis and design of physical-layer anonymous communications. This is a new topic of research with only a handful of prior works. The existing physical-layer anonymity schemes can be broadly classified into *strong-transmitter* and *strong-receiver* architectures, depending on the relative number of transmit and receive antennas. In the strong-transmitter case, where the number of transmit antennas exceeds that of the receiver, reliable

Y. Li, X. Zhou and N. Yang are with the School of Engineering, the Australian National University, Canberra, ACT 2601, Australia (e-mail: yu.li1@anu.edu.au; xiangyun.zhou@anu.edu.au; nan.yang@anu.edu.au). Part of this work was conducted while M. Tatar Mamaghani (e-mail: milad.tatarmamaghani@gmail.com) was previously with the Australian National University. This work was supported by the Australian Research Council’s Discovery Projects (DP220101318).

anonymous communication can be achieved solely through transmitter-side precoding by exploiting the excess spatial degrees of freedom (DoF) [22]. For this case, two classes of precoders have been developed: i) interference-suppression-based designs that employ transmitter-side phase equalization and ii) constructive-interference-based symbol-level precoders that steer signals into correct decision regions, thus eliminating the need for explicit equalization at either the transmitter or receiver. In contrast, the strong-receiver case, in which receive antennas outnumber transmit antennas, requires receiver-side combining to exploit the reception diversity as the transmitter-side precoding alone is insufficient to control the signal structure across all receive antennas [23], [24]. An early design for this case employed channel-independent equal-gain combining (EGC) with a single data stream to preserve anonymity under heterogeneous transmitter antenna configurations [23]. More recently, [24] investigated the multiplexing–diversity tradeoff and introduced alias-channel-based combiners to jointly exploit spatial multiplexing and reception diversity while maintaining anonymity. Specifically, the combiner was constructed from the averaged channel responses of the true transmitter and multiple alias users, implicitly treating them as equally likely during receiver-side transmitter detection. While these works differ in transceiver structure and signal processing design, they adopt channel state information (CSI) as the underlying feature for transmitter identification. Beyond CSI masking in [21]–[24], other physical-layer characteristics have been considered. For instance, joint masking of CSI and in-phase/quadrature (IQ) imbalance was explored as a means of enhancing physical-layer anonymity in [25].

To quantify physical-layer anonymity, several performance metrics have been established in the literature. The most commonly used metric is the detection error rate (DER), which measures the probability that the receiver fails to identify the active user. A larger DER indicates a higher level of anonymity. Complementarily, anonymity entropy was proposed to characterize the receiver’s uncertainty regarding the transmitter identity in a manner analogous to Shannon entropy [23], [26]. More general analytical frameworks based on detection-error exponents and divergence-based measures were introduced in [13], while closed-form DER expressions for specific systems were derived in [24], [26], [27]. These metrics provide a principled basis for analyzing anonymity performance and the fundamental tradeoff between anonymity and communication reliability.

Despite the merits of the aforementioned works, two important limitations still remain in the existing literature. First, to the best of our knowledge, all existing anonymous precoding designs assume *homogeneous* transmitter noise statistics across users, and hence neglect user-dependent distortion due to hardware impairments, which creates user-dependent noise statistics at the receiver that can be used for identification. Second, existing transmitter identification models are *symbol-unaware*, implicitly assuming that the adversary does not exploit decoded data symbols when performing identification. In practice, however, a receiver capable of reliable decoding can leverage symbol-dependent statistics to significantly enhance identification performance. The impact of such symbol-aware

transmitter identification on anonymous precoder design has not been systematically investigated. Addressing these limitations is essential for developing physical-layer anonymity mechanisms that remain robust against information-rich adversarial receivers.

## B. Our Contributions

To address the aforementioned limitations, this paper makes the following contributions:

- We introduce a *symbol-aware adversarial model* for physical-layer transmitter identification, in which a receiver exploits all available information, including reliably decoded data symbols, to enhance identification performance. Unlike existing physical-layer anonymity frameworks that rely on symbol-unaware detection models, we explicitly incorporate symbol-dependent statistics into the identification process and analyze their implications for the anonymous precoder design.
- We propose a *generalized physical-layer anonymity framework* that jointly accounts for CSI and transmitter noise statistics. By explicitly modeling heterogeneous transmitter noise statistics in both the identification model and the precoder design, the proposed framework addresses a critical and previously overlooked source of identity leakage and enables anonymity guarantees in more general network settings.
- We develop an *anonymous symbol-level precoding* scheme for a multi-user multiple-input-multiple-output (MU-MIMO) system that incorporates explicit anonymity constraints based on the Kullback-Leibler divergence (KLD) between transmitter hypotheses, while preserving reliable spatial multiplexing performance under symbol-aware identification. We consider a strong-receiver scenario and propose a *partitioned equal-gain combining* (P-EGC) architecture that enables reliable multi-stream reception without requiring transmitter-specific CSI, alias-channel construction, or the assumption of equal likelihood among the true and alias transmitters. The proposed P-EGC depends only on the antenna configuration and the number of data streams, making it compatible with scenarios where users exhibit unequal detectability at the receiver and robust to heterogeneous transmitter noise statistics.

## C. Organization and Notation

The remainder of this paper is organized as follows: Section II presents the system model. Section III introduces the transmitter detection strategy and the associated anonymity metrics. Section IV focuses on the anonymous communication design, including the proposed precoder, combiner architectures, and the corresponding optimization formulation. Simulation results and discussions are provided in Section V, followed by conclusions drawn in Section VI.

*Notation:* Unless otherwise stated, the following notation is used throughout the paper. Boldface lowercase and uppercase letters denote vectors and matrices, respectively. The operators  $(\cdot)^H$ ,  $(\cdot)^\dagger$ ,  $\|\cdot\|$ , and  $\|\cdot\|_F$  denote the conjugate

transpose, Moore–Penrose pseudo-inverse, Euclidean norm, and Frobenius norm, respectively. Trace and expectation are denoted by  $\text{tr}(\cdot)$  and  $\mathbb{E}[\cdot]$ , respectively. The natural logarithm is denoted by  $\ln(\cdot)$ . In addition,  $\mathcal{CN}(\mathbf{0}, \Sigma)$  represents a circularly symmetric complex Gaussian (CSCG) distribution with zero mean and covariance matrix  $\Sigma$ ,  $\mathbf{I}_n$  represents the  $n \times n$  identity matrix,  $\mathcal{O}(\cdot)$  represents the big-O notation, and  $\Re\{\cdot\}$  and  $\Im\{\cdot\}$  represent the real and imaginary parts, respectively.

## II. SYSTEM MODEL

We consider an uplink MU-MIMO system comprising  $K$  transmitting users and a single receiver acting as a central server. Each user is equipped with  $N_t$  transmit antennas, while the receiver employs  $N_r$  receive antennas. We assume  $N_r > N_t$ , which is a typical uplink scenario and is referred to as the strong-receiver scenario in the literature of physical-layer anonymous communications. The system operates under a collision-free time division multiple access (TDMA) protocol, such that one user is active in each timeslot.

In our considered system, user scheduling is governed by an anonymous access mechanism (e.g., randomized contention or coordination among transmitters) [28], and the resulting scheduling information is not revealed to the receiver. Consequently, although exactly one user transmits in each timeslot, the receiver does not know the identity of the active user, which is consistent with the standard physical-layer anonymous communication setting [21]–[26].

We adopt a semi-trustworthy receiver model, in which the receiver acts as a curious service provider that reliably decodes transmitted data while simultaneously attempting to infer the transmitter's identity. The purpose of physical-layer anonymous communication is to allow reliable decoding while preventing the receiver from successfully inferring the transmitter's identity based on the received signal. As in [21]–[26], it is assumed that all communication nodes have perfect knowledge of CSI.

### A. Signal Representation

Let  $k \in \mathcal{K} = \{1, 2, \dots, K\}$  be the index of the scheduled user for transmission. We adopt a block-fading model in which the channel remains constant throughout a transmission block and varies independently across blocks. We denote  $\mathbf{H}_k \in \mathbb{C}^{N_r \times N_t}$  as the channel matrix from the  $k^{\text{th}}$  user to the receiver and  $\mathbf{W}_k \in \mathbb{C}^{N_t \times N_s}$  as the associated precoding matrix, where  $N_s$  is the number of data streams such that  $N_s \leq N_t$ .

The received signal corresponding to the  $k^{\text{th}}$  user is expressed as

$$\mathbf{Y}_k = \mathbf{H}_k \mathbf{W}_k \mathbf{S} + \mathbf{N}_k, \quad (1)$$

where  $\mathbf{S} \in \mathbb{C}^{N_s \times L}$  is the transmitted symbol matrix over a block of length  $L$  and  $\mathbf{N}_k \in \mathbb{C}^{N_r \times L}$  represents the aggregated distortion observed at the receiver. Consistent with prior studies (e.g., [29], [30]), the combined effect of transmitter-induced hardware impairments and receiver noise is modeled as a user-dependent equivalent Gaussian disturbance, i.e.,  $\mathbf{N}_k \sim \mathcal{CN}(\mathbf{0}, \sigma_k^2 \mathbf{I}_{N_r L})$ , where  $\sigma_k^2$  denotes the effective noise power associated with user  $k$ .

**Remark 1.** *In practical systems, residual hardware impairments arising from non-ideal RF components such as power amplifiers, IQ modulators, oscillators, and digital-to-analog converters (DACs), persist despite calibration and compensation, and their severity may vary across devices [29]–[31]. These transmitter-originated distortions can have a non-negligible impact on the received signal, particularly in MIMO systems employing sensitive detection schemes [32]. As a result, transmitter hardware quality directly influences the statistical property of the received signal and constitutes an important source of identity leakage in physical-layer anonymous communications.*

## III. TRANSMITTER DETECTION STRATEGY

In this section, we investigate the receiver-side detection mechanism used to evaluate transmitter anonymity performance. We consider a scenario in which the receiver seeks to identify the active user based on the observed signal  $\mathbf{Y}$  and the known CSI of all users. Since the transmitter identity is anonymous, the received signal in (1) is denoted by  $\mathbf{Y}$  without a user-specific subscript. The transmitter identification problem can be considered as a multiple-hypothesis testing (MHT) formulation, expressed as

$$\begin{cases} \mathcal{H}_1 & : \mathbf{Y} = \mathbf{H}_1 \mathbf{W}_1 \mathbf{S} + \mathbf{N}_1, \\ \mathcal{H}_2 & : \mathbf{Y} = \mathbf{H}_2 \mathbf{W}_2 \mathbf{S} + \mathbf{N}_2, \\ & \vdots \\ \mathcal{H}_K & : \mathbf{Y} = \mathbf{H}_K \mathbf{W}_K \mathbf{S} + \mathbf{N}_K, \end{cases} \quad (2)$$

where the hypothesis set  $\mathcal{H} = \{\mathcal{H}_1, \mathcal{H}_2, \dots, \mathcal{H}_K\}$  represents  $K$  possible candidates for the originating transmitter and  $\mathbf{H}_i$  and  $\mathbf{W}_i$  denote the channel and precoder of user  $i \in \mathcal{K}$ , respectively.

Two major methodologies exist for composite hypothesis testing: the Bayesian approach and the generalized likelihood ratio test (GLRT) [33]. For the MHT problem considered here, we adopt the GLRT framework, as it does not require prior distributions on the unknown precoding matrices and is therefore more suitable and robust for anonymous communication scenarios. The first step in GLRT is to obtain the maximum-likelihood estimate of the unknown parameters in the linear model given in (2). Since the objective of the anonymous communication system is to guarantee transmitter anonymity while preserving reliable communication, the transmitted symbols must be correctly decoded at the receiver. Consequently, when user identification is performed after decoding, the symbol matrix  $\mathbf{S}$  can be treated as known. Under this assumption, the only remaining unknown parameter within each hypothesis is the precoding matrix employed by the corresponding user.

If the actual transmitter is the  $k^{\text{th}}$  user, then the hypothesis  $\mathcal{H}_k$  is correct, and the actual transmitted signal is  $\mathbf{Y} = \mathbf{H}_k \mathbf{W}_k \mathbf{S} + \mathbf{N}_k$ . Under  $\mathcal{H}_k$ , the maximum-likelihood estimate of the precoder is

$$\widehat{\mathbf{W}}_k = \mathbf{H}_k^\dagger \mathbf{Y} \mathbf{S}^\dagger,$$

where  $\mathbf{H}_k^\dagger = (\mathbf{H}_k^H \mathbf{H}_k)^{-1} \mathbf{H}_k^H$  and  $\mathbf{S}^\dagger = \mathbf{S}^H (\mathbf{S} \mathbf{S}^H)^{-1}$ . Similarly, under incorrect hypothesis  $\mathcal{H}_i$ , the estimated precoder becomes  $\widehat{\mathbf{W}}_i = \mathbf{H}_i^\dagger \mathbf{Y} \mathbf{S}^\dagger$ . Using these estimates, the

reconstructed received signals under the correct and incorrect hypotheses are

$$\widehat{\mathbf{Y}}_k = \mathbf{H}_k \widehat{\mathbf{W}}_k \mathbf{S} = \mathbf{H}_k \mathbf{W}_k \mathbf{S} + \mathbf{H}_k \mathbf{H}_k^\dagger \mathbf{N}_k \mathbf{S}^\dagger \mathbf{S} \quad (3)$$

and

$$\widehat{\mathbf{Y}}_i = \mathbf{H}_i \widehat{\mathbf{W}}_i \mathbf{S} = \mathbf{H}_i \mathbf{H}_i^\dagger (\mathbf{H}_k \mathbf{W}_k \mathbf{S} + \mathbf{N}_k) \mathbf{S}^\dagger \mathbf{S}, \quad (4)$$

respectively.

Accordingly, the probability density functions (PDFs) of received signal  $\mathbf{Y}$  under each hypothesis are given by

$$\begin{aligned} \mathcal{H}_1 : p(\mathbf{Y}; \widehat{\mathbf{W}}_1, \mathcal{H}_1) &= \frac{1}{(\pi\sigma_1^2)^{N_r L}} \exp\left(-\frac{1}{\sigma_1^2} \|\mathbf{Y} - \widehat{\mathbf{Y}}_1\|_F^2\right), \\ \mathcal{H}_2 : p(\mathbf{Y}; \widehat{\mathbf{W}}_2, \mathcal{H}_2) &= \frac{1}{(\pi\sigma_2^2)^{N_r L}} \exp\left(-\frac{1}{\sigma_2^2} \|\mathbf{Y} - \widehat{\mathbf{Y}}_2\|_F^2\right), \\ &\vdots \\ \mathcal{H}_k : p(\mathbf{Y}; \widehat{\mathbf{W}}_k, \mathcal{H}_k) &= \frac{1}{(\pi\sigma_k^2)^{N_r L}} \exp\left(-\frac{1}{\sigma_k^2} \|\mathbf{Y} - \widehat{\mathbf{Y}}_k\|_F^2\right). \end{aligned} \quad (5)$$

Under the GLRT framework, the receiver selects hypothesis  $\mathcal{H}_k$  if its likelihood  $p(\mathbf{Y}; \widehat{\mathbf{W}}_k, \mathcal{H}_k)$  is the largest among all candidates. In maximum-likelihood estimation (MLE) and hypothesis testing, it is common to employ the log-likelihood as the test statistic due to its monotonicity and numerical stability. Accordingly, we define

$$T_k = \ln p(\mathbf{Y}; \widehat{\mathbf{W}}_k, \mathcal{H}_k)$$

as the test statistic under the hypothesis  $\mathcal{H}_k$  such that the receiver decides in favor of the hypothesis associated with the maximal  $T_k$ .

#### A. Anonymity Metric: Detection Error Rate

In this paper, we evaluate transmitter anonymity through the probability that the receiver fails to correctly identify the active user. Consistent with existing studies on physical-layer anonymity (e.g., [24], [26]), we adopt the DER as the anonymity metric. To characterize the DER, we examine the statistical behavior of the detection test statistic  $T$  under the correct and incorrect hypotheses.

Suppose the  $k^{\text{th}}$  user is the actual transmitter, implying that the true hypothesis is  $\mathcal{H}_k$ , while any  $\mathcal{H}_i$  ( $\forall i \in \mathcal{K}$  and  $i \neq k$ ) represents an incorrect hypothesis. For analytical tractability, the corresponding log-likelihood test statistics can be written as

$$\begin{aligned} T_k &= \ln p(\mathbf{Y}; \widehat{\mathbf{W}}_k, \mathcal{H}_k) \\ &= -N_r L \ln(\pi\sigma_k^2) - \frac{1}{\sigma_k^2} \|\widehat{\mathbf{Y}}_k - \mathbf{Y}\|_F^2 \end{aligned} \quad (6a)$$

and

$$\begin{aligned} T_i &= \ln p(\mathbf{Y}; \widehat{\mathbf{W}}_i, \mathcal{H}_i) \\ &= -N_r L \ln(\pi\sigma_i^2) - \frac{1}{\sigma_i^2} \|\widehat{\mathbf{Y}}_i - \mathbf{Y}\|_F^2. \end{aligned} \quad (6b)$$

Since the receiver identifies the transmitting user based on the largest test statistic, an incorrect detection occurs when

$T_i > T_k$  for some  $i \neq k$ . To characterize this event, we introduce the difference random variable  $D_i = T_i - T_k$ , which measures the *relative likelihood* of an incorrect hypothesis compared with the true one. Therefore, the DER can be equivalently written as

$$\text{DER} = 1 - \Pr(D_i < 0, \forall i \neq k). \quad (7)$$

Computing this probability requires the joint distribution of the set  $\{D_i\}_{i \neq k}$ . However, the variables  $D_i$  are mutually dependent because each term includes the common term  $T_k$ . In addition, the test statistics  $T_k$  and  $T_i$  are quadratic forms of CSCG noise, and thus follow non-Gaussian generalized chi-square-type distributions. As a result, the joint cumulative distribution function (CDF) involves high-dimensional integrals over dependent, non-Gaussian random variables, rendering an exact closed-form expression for the DER analytically intractable. Nevertheless, the DER metric can be evaluated numerically through Monte-Carlo simulations.

**Remark 2.** *If we approximate  $T_k$  and  $T_i$  as Gaussian distributed, then with both mean and variance specified, the distributions would be fully characterized, allowing a closed-form approximation of the anonymity metric. In this case, for each non-transmitting user  $i$ , the difference variable  $D_i = T_i - T_k$  would also be Gaussian, and quantities such as  $\Pr(D_i > 0) = 1 - \Pr(D_i < 0)$  could be directly evaluated via the Gaussian CDF. If the variables  $\{D_i\}_{i \neq k}$  were further assumed independent, the overall anonymity metric can be expressed as  $1 - \prod_{i \neq k} \Pr(D_i < 0)$ .*

*However, this approach relies on several strong assumptions and approximations. In practice, these assumptions introduce a considerable gap between the theoretical estimate and the actual behavior in our scenario.  $\|\widehat{\mathbf{Y}}_k - \mathbf{Y}\|_F^2$  and  $\|\widehat{\mathbf{Y}}_i - \mathbf{Y}\|_F^2$  in test statistics, and consequently  $D_i$ , are non-Gaussian because they involve quadratic forms of CSCG noise, and the variables  $\{D_i\}_{i \neq k}$  are mutually dependent through the shared term  $T_k$ . These issues make it impossible to obtain the joint distribution of  $\{D_i\}_{i \neq k}$  in closed form, making a closed-form evaluation of DER analytically intractable.*

#### B. Anonymity Metric: Information-theoretic Metric

To gain analytical insight into the factors influencing anonymity, we adopt an information-theoretic perspective. Specifically, we examine the KLD [34] between the distributions of the received signal  $\mathbf{Y}$  under the true hypothesis  $p_k \triangleq p(\mathbf{Y}; \widehat{\mathbf{W}}_k, \mathcal{H}_k)$  and false hypothesis  $p_i \triangleq p(\mathbf{Y}; \widehat{\mathbf{W}}_i, \mathcal{H}_i)$ , defined as

$$D_{\text{KL}}(p_k \| p_i) = \mathbb{E} \left[ \ln \frac{p_k(\mathbf{Y})}{p_i(\mathbf{Y})} \right] = \int p_k(\mathbf{Y}) \ln \frac{p_k(\mathbf{Y})}{p_i(\mathbf{Y})} d\mathbf{Y}, \quad (8)$$

where the expectation is taken with respect to (w.r.t.) the true distribution  $p_k(\mathbf{Y})$  under hypothesis  $\mathcal{H}_k$ . The KLD quantifies how distinguishable the received signals are between the two cases, i.e., a larger KLD indicates that the two distributions  $p_k$  and  $p_i$  are more distinguishable, making correct detection easier for the receiver. In the following, we present Lemma 1 to analytically quantify the KLD in our anonymous communication system.

**Lemma 1.** *The KLD between the distributions  $p_k$  and  $p_i$ , defined in (8), admits the following closed-form expression:*

$$\begin{aligned} D_{\text{KL}}(p_k \| p_i) &= \mathbb{E}[T_k] - \mathbb{E}[T_i] = N_r L \ln \left( \frac{\sigma_i^2}{\sigma_k^2} \right) \\ &+ \left( 1 - \frac{\sigma_k^2}{\sigma_i^2} \right) (N_s N_t - N_r L) \\ &+ \frac{1}{\sigma_i^2} \left[ \text{tr} \left( \mathbf{S}^H \mathbf{W}_k^H \mathbf{H}_k^H \mathbf{H}_k \mathbf{W}_k \mathbf{S} \right) \right. \\ &\left. - \text{tr} \left( \mathbf{S}^H \mathbf{W}_k^H \mathbf{H}_k^H \mathbf{H}_i \mathbf{H}_i^\dagger \mathbf{H}_k \mathbf{W}_k \mathbf{S} \right) \right]. \end{aligned} \quad (9)$$

*Proof.* See Appendix A.  $\blacksquare$

Recalling that  $D_i = T_i - T_k$ , the KLD in Lemma 1 can be written as  $D_{\text{KL}}(p_k \| p_i) = -\mathbb{E}[D_i]$ . Thus, a larger expected value  $\mathbb{E}[D_i]$  corresponds to a smaller KLD, meaning that the two hypotheses become less distinguishable. If we define each user other than the true transmitter as an alternative user, then the pairwise anonymity between the true transmitter and any alternative user  $i$  can be given by  $\mathbb{E}[D_i]$ .

### C. Transmitter Anonymity Constraint

In this subsection, we quantify an anonymity constraint for the transmitter detection strategy.

Here, we refer to the non-transmitting users (indexed by  $\forall i \neq k$ ) as the *alias* users whose channels are intentionally exploited by the transmitter to disguise the true transmission. We first define the alias-candidate set for the  $k^{\text{th}}$  user as  $\mathcal{A}_k^{\text{cand}} = \{1, \dots, K\} \setminus \{k\}$ , which contains all non-transmitting users whose channels may be exploited for anonymity. From the candidate set  $\mathcal{A}_k^{\text{cand}}$ , the transmitter selects a subset  $\mathcal{A} \subseteq \mathcal{A}_k^{\text{cand}}$  as the index set of the selected alias users, where  $|\mathcal{A}| = a, 1 \leq a \leq K - 1$ , represents the number of aliases considered by the receiver for transmitter detection. We note that the receiver selects the user corresponding to the largest test statistic  $T_i$ . To achieve pairwise anonymity between the true user and each alias, the distribution of the received signal  $\mathbf{Y}$  under the alias hypothesis  $\mathcal{H}_i$  should closely resemble its distribution under the true hypothesis  $\mathcal{H}_k$ . From Lemma 1, we see that the pairwise anonymity can be quantified by the negative KLD between  $p_k(\mathbf{Y})$  and  $p_i(\mathbf{Y})$ . To enhance anonymity, one can minimize this divergence, which is equivalent to maximizing its negative value,  $\mathbb{E}[D_i] = \mathbb{E}[T_i] - \mathbb{E}[T_k]$ . To achieve this aim,  $\mathbb{E}[D_i]$  can be expressed as

$$\mathbb{E}[D_i] = E_{\text{const}} - \frac{1}{\sigma_i^2} \Delta, \quad (10)$$

where

$$E_{\text{const}} = N_r L \ln \left( \frac{\sigma_k^2}{\sigma_i^2} \right) + \left( 1 - \frac{\sigma_k^2}{\sigma_i^2} \right) (N_r L - N_s N_t) \quad (11)$$

and

$$\begin{aligned} \Delta &= \text{tr} \left( \mathbf{S}^H \mathbf{W}_k^H \mathbf{H}_k^H \mathbf{H}_k \mathbf{W}_k \mathbf{S} \right) \\ &- \text{tr} \left( \mathbf{S}^H \mathbf{W}_k^H \mathbf{H}_k^H \mathbf{H}_i \mathbf{H}_i^\dagger \mathbf{H}_k \mathbf{W}_k \mathbf{S} \right). \end{aligned} \quad (12)$$

It follows directly from (10) that maximizing the pairwise anonymity measure  $\mathbb{E}[D_i]$  is equivalent to minimizing the trace-difference term  $\Delta$ , which can be rewritten as

$$\begin{aligned} \Delta &= \text{tr} \left( \mathbf{S}^H \mathbf{W}_k^H \mathbf{H}_k^H (\mathbf{I}_{N_r} - \mathbf{H}_i \mathbf{H}_i^\dagger) \mathbf{H}_k \mathbf{W}_k \mathbf{S} \right) \\ &\stackrel{(a)}{=} \text{tr} \left( \mathbf{S}^H \mathbf{W}_k^H \mathbf{H}_k^H (\mathbf{I}_{N_r} - \mathbf{H}_i \mathbf{H}_i^\dagger)^2 \mathbf{H}_k \mathbf{W}_k \mathbf{S} \right), \quad (13) \\ &\stackrel{(b)}{=} \| (\mathbf{I}_{N_r} - \mathbf{H}_i \mathbf{H}_i^\dagger) \mathbf{H}_k \mathbf{W}_k \mathbf{S} \|_F^2. \end{aligned}$$

where (a) follows from the idempotent property of the projection matrix  $\mathbf{I}_{N_r} - \mathbf{H}_i \mathbf{H}_i^\dagger$  and (b) follows from the identity  $\text{tr}(\mathbf{A}^H \mathbf{A}) = \|\mathbf{A}\|_F^2$ .

Since  $\Delta \geq 0$ , driving this term toward zero provides the most favorable condition for improving anonymity, as it minimizes the distinguishability between the true and alias hypotheses. However, enforcing  $\Delta = 0$  is overly restrictive and would impose a severe constraint on the precoder, compromising communication reliability. To balance anonymity with communication quality, we introduce a small relaxation parameter  $\epsilon$  to allow a controlled, non-zero trace-difference, with smaller values enforcing stronger anonymity. The anonymity constraint at the symbol level is thus given by

$$\boxed{\| (\mathbf{I}_{N_r} - \mathbf{H}_i \mathbf{H}_i^\dagger) \mathbf{H}_k \mathbf{W}_k \mathbf{s}^\ell \|_2^2 \leq \epsilon, \quad \forall i \neq k, \ell} \quad (14)$$

where  $\mathbf{s}^\ell$  denotes the transmit symbol vector of the  $k^{\text{th}}$  user at timeslot  $\ell$ .

**Remark 3.** *The condition in (14) follows the theoretical definition of pairwise anonymity, which is formulated w.r.t. any non-transmitting user ( $\forall i \neq k$ ). This definition specifies how pairwise anonymity is ensured between the true user and an arbitrary non-transmitting user, but does not require that the constraint be enforced for all such users in practice. Since imposing all  $K - 1$  pairwise constraints would overly restrict the precoding space and noticeably degrade communication reliability, the subsequent design enforces this constraint only on a selected alias subset  $\mathcal{A}$ .*

## IV. ANONYMOUS COMMUNICATION DESIGN

In an anonymous communication framework, despite being aware of the set of all CSI, the receiver must not be able to associate the received signal with the channel of the actual transmitter. To enable user-agnostic signal combining and reliable demodulation, we employ a constructive-interference (CI) precoder at the transmitter. The CI precoder pre-aligns the transmitted symbol phases so that, after spatial combining, the resulting received signal can be directly demodulated without requiring any CSI-dependent equalization at the receiver. In the following, we first review the CI precoding principles (see [35] and references therein for further details) and then present our receiver combining scheme and anonymous precoder design tailored for the considered system.

### A. Constructive Interference Precoder

In conventional systems, phase equalization is essential for exploiting spatial diversity in the sense that without aligning the signal phases across antennas, the received components

cannot be coherently combined. However, in the anonymous setting, the receiver is not allowed to design a CSI-based equalizer to perform such phase alignment. Specifically, in the strong-receiver scenario ( $N_r > N_t$ ), where the transmitter has limited spatial DoF, the transmitter cannot independently control the phase of each receive antenna. By pre-adjusting the transmitted signal phases, the CI precoder fulfills this role at the transmitter side, ensuring that the post-combined received symbols for each data stream remain correctly aligned for demodulation while preserving user anonymity. In other words, the CI precoding aims to actively shape the multi-stream interference inasmuch as it reinforces, rather than distorts, the desired signal components. Instead of suppressing interference, the precoder exploits the known symbol phases and the available CSI to steer the superimposed signal at the receiver toward the constructive region of the constellation. As a result, the post-combined received symbols are naturally aligned with their target directions, enhancing detection reliability without requiring CSI-based phase equalization. This approach effectively converts interference power into useful signal energy, improving both energy efficiency and noise resilience. Therefore, the CI precoding plays a crucial role in enabling anonymous communication under the strong-receiver scenario ( $N_r > N_t$ ). In this work, we will design the appropriate CI precoder w.r.t. a new receiver combiner structure, introduced in the sequel, for anonymous communication.

### B. Partitioned Equal-Gain Combiner

Conventional combining schemes such as a maximum-ratio combiner, widely used in non-anonymous MIMO settings, are not suitable for anonymous communications, because they inherently rely on user-specific CSI. In light of this, we propose a *partitioned equal-gain combining* (P-EGC) scheme, which is applied at the receiver to exploit spatial diversity without relying on user-specific CSI. Specifically, the key idea of our P-EGC scheme is to partition receive antennas into several groups according to the number of transmitted data streams, then combine the signals received within each group corresponding to the same data stream with equal weights, while avoiding any combining across different antenna groups. This approach enables the receiver to benefit from spatial diversity in a user-agnostic manner, without relying on the transmitter's identity or channel characteristics.

The detailed combining process can be described as follows. For any arbitrary number of receive antennas  $N_r$ , the antennas are divided into  $N_s$  disjoint subsets such that  $N_r > N_s$ <sup>1</sup>. Let  $\mathcal{S}_m$  denote the subset of receive antennas assigned to the  $m^{\text{th}}$  data stream with  $|\mathcal{S}_m|$  being its cardinality. We denote  $y_{k,j}^\ell$  as

<sup>1</sup>Since  $N_s$  data streams are sent using  $N_t$  transmit antennas, in the simplest case ( $N_s = 1$ ), where the transmitter sends only one data stream, the receiver naturally achieves full diversity without the need to partition the receive antennas into subsets. As such, the precoder essentially functions as a vector ( $\mathbf{w}_k \in \mathbb{C}^{N_t \times 1}$ ). However, considering multiplexing gain at the transmitter, the receiver must partition the receive antennas into subsets based on the number of multiplexed data streams. If the number of receive antennas is not an integer multiple of the number of streams, the antenna allocation among data streams may vary slightly, but this does not affect our design process.

the received signal at the  $j^{\text{th}}$  antenna, where  $j \in \mathcal{S}_m$ , from the  $k^{\text{th}}$  user at timeslot  $\ell$ , which can be expressed as

$$y_{k,j}^\ell = \mathbf{h}_{k,j} \sum_{n=1}^{N_s} \mathbf{w}_{k,n}^\ell s_{k,n}^\ell + n_{k,j}^\ell, \quad (15)$$

where  $\mathbf{h}_{k,j} \in \mathbb{C}^{1 \times N_t}$  is the channel vector from the  $k^{\text{th}}$  transmitter to the  $j^{\text{th}}$  receive antenna in  $\mathcal{S}_m$ , and  $\mathbf{w}_{k,n}^\ell \in \mathbb{C}^{N_t \times 1}$  is the precoder for the  $n^{\text{th}}$  data stream at timeslot  $\ell$ . Let  $s_{k,n}^\ell \in \mathbb{C}$  denote the symbol of the  $n^{\text{th}}$  data stream transmitted at timeslot  $\ell$  and  $n_{k,j}^\ell \sim \mathcal{CN}(0, \sigma_k^2)$  denote the noise in this received signal at the  $j^{\text{th}}$  receive antenna. Applying the P-EGC to all the received signals from  $\mathcal{S}_m$ , the combined signal can be expressed as

$$\begin{aligned} r_{k,m}^\ell &= \sum_{j \in \mathcal{S}_m} y_{k,j}^\ell \\ &= \mathbf{c}_{k,m} \mathbf{H}_{k,m} \mathbf{W}_k^\ell \mathbf{s}^\ell + \tilde{n}_{k,m}^\ell, \quad \forall k, m, \ell, \end{aligned} \quad (16)$$

where  $\mathbf{H}_{k,m} = [\mathbf{h}_{k,j}]_{j \in \mathcal{S}_m} \in \mathbb{C}^{|\mathcal{S}_m| \times N_t}$  is the submatrix of the full channel  $\mathbf{H}_k$  corresponding to antennas in  $\mathcal{S}_m$ , and  $\mathbf{c}_{k,m} \in \mathbb{C}^{1 \times |\mathcal{S}_m|}$  denotes the equal gain combiner for the  $m^{\text{th}}$  data stream, which is assumed to be an all-ones row vector, i.e.,  $\mathbf{c}_{k,m} = \mathbf{1}^{1 \times |\mathcal{S}_m|}$ . In addition,  $\mathbf{W}_k^\ell = [\mathbf{w}_{k,1} \ \mathbf{w}_{k,2} \ \cdots \ \mathbf{w}_{k,N_s}] \in \mathbb{C}^{N_t \times N_s}$  is the precoder for all data streams at timeslot  $\ell$ ,  $\mathbf{s}^\ell$  denotes the transmit symbol vector across all data streams, and  $\tilde{n}_{k,m}^\ell \triangleq \mathbf{c}_{k,m} \mathbf{n}_{k,m}^\ell$  indicates the aggregated noise after combining, where  $\mathbf{n}_{k,m}^\ell = [n_{k,j}^\ell]_{j \in \mathcal{S}_m} \in \mathbb{C}^{|\mathcal{S}_m| \times 1}$  is the noise vector corresponding to the antenna subset  $\mathcal{S}_m$ . Each  $n_{k,j}^\ell$  is modeled as an independent and identically distributed (i.i.d.) CSCG random variable. Thus, the effective noise for each data stream follows  $\tilde{n}_{k,m}^\ell \sim \mathcal{CN}(0, \sigma_{\text{eff}}^2)$ , such that

$$\sigma_{\text{eff}}^2 = \mathbb{E}(|\tilde{n}_{k,m}^\ell|^2) = \|\mathbf{c}_{k,m}\|_2^2 \sigma_k^2 = |\mathcal{S}_m| \sigma_k^2.$$

For all  $N_s$  data streams, the P-EGC can be expressed in a compact block-diagonal form as

$$\mathbf{C}_k = \begin{bmatrix} \mathbf{c}_{k,1} & 0 & \cdots & 0 \\ 0 & \mathbf{c}_{k,2} & \cdots & 0 \\ \vdots & \vdots & \ddots & \vdots \\ 0 & 0 & \cdots & \mathbf{c}_{k,N_s} \end{bmatrix}, \quad (17)$$

where each diagonal element is a row vector of all-ones, representing the combiner for the subset of receive antennas for each data stream. The size of these combiners depends on the number of antennas in each group. For example, for the  $m^{\text{th}}$  data stream,  $|\mathcal{S}_m|$  antennas are allocated for reception. Thus, the overall combiner  $\mathbf{C}_k$  is a matrix of size  $N_s \times N_r$ . Since the P-EGC depends only on the antenna grouping,  $\mathbf{C}_k$  does not vary with the timeslot index  $\ell$ . As a result, based on the symbol-level precoder  $\mathbf{W}_k^\ell$ , the post-combined received signal vector at timeslot  $\ell$  can be expressed as

$$\tilde{\mathbf{r}}_k^\ell = \mathbf{C}_k (\mathbf{H}_k \mathbf{W}_k^\ell \mathbf{s}^\ell + \mathbf{n}_k^\ell), \quad \forall k, \ell, \quad (18)$$

where  $\tilde{\mathbf{r}}_k^\ell = [r_{k,1}^\ell, \dots, r_{k,N_s}^\ell]^T \in \mathbb{C}^{N_s \times 1}$  is the post-combined outputs of all streams and  $\mathbf{n}_k^\ell = [n_{k,1}^\ell, \dots, n_{k,N_r}^\ell]^T \in \mathbb{C}^{N_r \times 1}$  is the received noise vector.

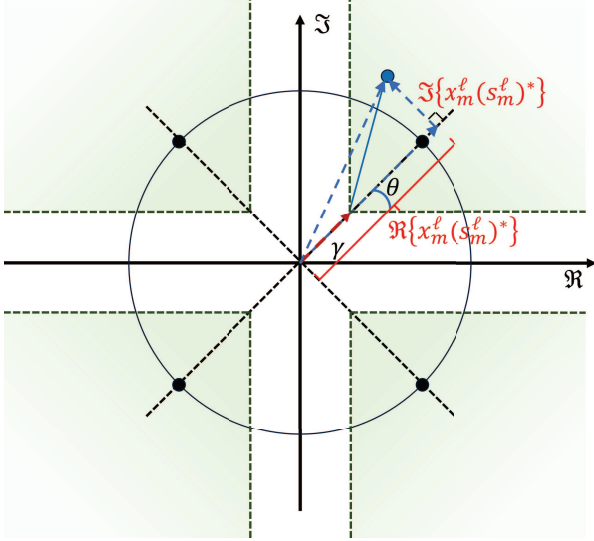


Fig. 1. Illustration of CI precoding for QPSK modulation. The green area represents the constructive decision region and the black points denote the reference constellation symbols. The parameter  $\gamma$  indicates the minimum in-phase distance from the origin. The blue point corresponds to a received symbol  $x_m^\ell$  on stream  $m$  at timeslot  $\ell$ , with  $s_m^\ell$  denoting the corresponding target constellation symbol. After rotating the point by the negative phase of the first-quadrant reference symbol, the rotated point lies in the constructive region if the ratio between its imaginary and real components remains within the  $\pm \tan \theta$  boundaries, where  $\theta = 45^\circ$  for QPSK.

### C. Anonymous Precoding Requirements

In this subsection, we specify the CI requirement used in the anonymous precoder design. By combining the CI principle with the P-EGC model introduced earlier, we express the geometric condition that the post-combined received symbol must satisfy in order to achieve constructive interference, which will be used as a constraint in the subsequent design problem.

In this work, we consider the quadrature phase shift keying (QPSK) modulation for the signal vector as a representative example of constellations commonly adopted in symbol-level CI precoding studies [22], [35]–[37]. In QPSK, each transmitted symbol lies in one of the four quadrants of the complex plane, and the decision boundaries are the real and imaginary axes. The goal of CI precoding is to ensure that the post-combined received signal of each data stream is pushed deeper into the correct quadrant, away from these decision boundaries<sup>2</sup>.

Following our P-EGC receiver model, outlined in Section IV-B, the combined received signal (16) can be rewritten as

$$r_{k,m}^\ell = \alpha_{k,m}^\ell \mathbf{s}^\ell + \tilde{n}_{k,m}^\ell, \quad \forall k, m, \ell, \quad (19)$$

where  $\alpha_{k,m}^\ell \triangleq \mathbf{c}_{k,m} \mathbf{H}_{k,m} \mathbf{W}_k^\ell$ . To ensure correct detection, the signal component  $\alpha_{k,m}^\ell \mathbf{s}^\ell$  (ignoring the noise) must lie within the decision region. Geometrically, for a QPSK symbol  $s_{k,m}^\ell$  located on the unit circle with phase  $\phi_{k,m}^\ell$ , the constructive region corresponds to the angular sector  $\phi_{k,m}^\ell \pm \theta$ , where  $\theta =$

<sup>2</sup>Although our work specifically considers the QPSK modulation, the CI precoding framework can be generalized to higher-order constellations such as M-QAM and M-PAM, by redefining the constructive regions around constellation points [38], [39]. Such extensions are left as future works.

$\pi/4$ . In the CI scheme, the constellation is properly rotated so that the desired symbol lies on the positive real axis. This can be equivalently achieved by multiplying the noise-less term  $\alpha_{k,m}^\ell \mathbf{s}^\ell$  with the complex-conjugate of the symbol, subject to the following conditions:

$$\Re \{ \alpha_{k,m}^\ell \mathbf{s}^\ell (s_{k,m}^\ell)^* \} \geq \gamma, \quad \forall k, m, \quad (20a)$$

$$\begin{aligned} & |\Im \{ \alpha_{k,m}^\ell \mathbf{s}^\ell (s_{k,m}^\ell)^* \} | \\ & \leq \tan \theta (\Re \{ \alpha_{k,m}^\ell \mathbf{s}^\ell (s_{k,m}^\ell)^* \} - \gamma), \quad \forall k, m, \end{aligned} \quad (20b)$$

where  $\gamma > 0$  denotes the required minimum in-phase distance from the origin (a.k.a. constructive margin, which is proportional to the Euclidean decision margin), representing the guaranteed constructive amplitude of the received symbol. The real part in (20a) corresponds to the in-phase projection of the rotated received symbol, i.e., the component that pushes the symbol away from the decision boundaries and thus contributes to reliable detection. Meanwhile, (20b) confines the symbol within the constructive angular sector. By noting that the right-hand side of (20b) is nonnegative only when  $\Re \{ \cdot \} \geq \gamma$ , we find that (20a) is satisfied when (20b) holds. Therefore, the two inequalities can be combined into a single constraint that jointly captures both the IQ requirements as

$$\boxed{\frac{|\Im \{ \alpha_{k,m}^\ell \mathbf{s}^\ell (s_{k,m}^\ell)^* \} |}{\Re \{ \alpha_{k,m}^\ell \mathbf{s}^\ell (s_{k,m}^\ell)^* \} - \gamma} \leq \tan \theta, \quad \forall k, m.} \quad (21)$$

Constraint (21) ensures that the post-combined received symbol  $\mathbf{r}_{k,m}^\ell = \alpha_{k,m}^\ell \mathbf{s}^\ell$  lies in the constructive region of its target constellation point, henceforth turning multi-stream interference into beneficial one for detection performance improvement.

An illustrative example of the above CI precoding applied to QPSK is provided in Fig. 1. In this figure, the blue point represents an example of the received symbol, denoted by  $x_m^\ell$ . The dashed  $45^\circ$  line indicates the direction of the reference constellation point in the first quadrant, along which CI aims to push the received symbol into the constructive region. After rotating the received signal by the negative phase of the reference symbol, this  $45^\circ$  line aligns with the real axis. In this rotated domain, the real part corresponds to the component along the desired symbol direction, whereas the imaginary part represents the deviation from that direction. To ensure that the received symbol lies within the constructive region, the geometric relationship between its real and imaginary parts must satisfy (21).

With the CI constraint established, we now turn to how communication reliability is quantified under this framework. Under the CI precoding framework, multi-stream interference is aligned with the desired symbol direction and thus becomes a useful power contribution. Accordingly, the post-combining signal-to-disturbance ratio (SDR) for the  $m^{\text{th}}$  data stream of the  $k^{\text{th}}$  user can be calculated as

$$\begin{aligned} \Gamma_{k,m} &= \frac{\| \sum_{j \in \mathcal{S}_m} \mathbf{h}_{k,j} (\sum_{n=1}^{N_s} \mathbf{w}_{k,n}^\ell \mathbf{s}_{k,n}^\ell) \|^2}{\| \sum_{j \in \mathcal{S}_m} n_{k,j}^\ell \|^2} \\ &= \frac{\| \mathbf{c}_{k,m} \mathbf{H}_{k,m} \mathbf{W}_k^\ell \mathbf{s}^\ell \|^2}{|\mathcal{S}_m| \sigma_k^2}, \quad \forall k, m. \end{aligned} \quad (22)$$

This expression characterizes the resulting post-combining reliability, whereas the optimization is carried out w.r.t. the guaranteed threshold  $\Gamma_{\text{th}}$  through the CI margin  $\gamma$ .

---

**Algorithm 1** Anonymous Precoding Algorithm
 

---

**Input:** Channel set  $\mathbf{H} = \{\mathbf{H}_1, \dots, \mathbf{H}_K\}$ , symbol matrix  $\mathbf{S}$ , transmitting user index  $k$ , total transmit power  $p_{\text{tot}}$ , noise variances  $\{\sigma_i^2\}_{i=1}^K$ , number of alias channels  $a$ , and relaxation parameter  $\epsilon$ .

- 1: Construct the alias-candidate set  $\mathcal{A}_k^{\text{cand}} = \{1, \dots, K\} \setminus \{k\}$ .
- 2: Randomly select  $a$  users from  $\mathcal{A}_k^{\text{cand}}$  to form the alias set  $\mathcal{A}$ .
- 3: Compute the combining matrix  $\mathbf{C}_k$  using (17).
- 4: Construct the CI constraint according to (21).
- 5: Construct the anonymity constraint using the relaxation parameter  $\epsilon$  according to (14).
- 6: Solve optimization problem P2 using CVX.

**Output:** Precoding matrix  $\mathbf{W}_k$ , constructive margin  $\gamma$ , and combining matrix  $\mathbf{C}_k$ .

---

#### D. Design Problem and Solution

Building on the proposed P-EGC scheme at the receiver and the CI precoding at the transmitter, we now focus on designing anonymous precoders  $\{\mathbf{W}_k^\ell\}_{\ell=1}^L$  to jointly enhance communication reliability and enforce transmitter anonymity. For each timeslot  $\ell$ , we introduce  $\Gamma^\ell$  as a *common worst-stream* SDR guarantee, i.e., the SDR of every data stream is constrained to be no smaller than  $\Gamma^\ell$ . To ensure uniform performance over time, we maximize the worst-timeslot guarantee, which yields the following max–min formulation:

$$\begin{aligned} \text{P0: } & \max_{\{\mathbf{W}_k^\ell, \Gamma^\ell\}_{\ell=1}^L, \Gamma} \Gamma \\ \text{s.t. } & \frac{\|\mathbf{c}_{k,m} \mathbf{H}_{k,m} \mathbf{W}_k^\ell \mathbf{s}^\ell\|^2}{|\mathcal{S}_m| \sigma_k^2} \geq \Gamma^\ell, \quad \forall m, \forall \ell, \end{aligned} \quad (23a)$$

$$\begin{aligned} & |\Im \{ \mathbf{c}_{k,m} \mathbf{H}_{k,m} \mathbf{W}_k^\ell \mathbf{s}^\ell (s_{k,m}^\ell)^* \}| \leq \tan \theta \\ & \times \left( \Re \{ \mathbf{c}_{k,m} \mathbf{H}_{k,m} \mathbf{W}_k^\ell \mathbf{s}^\ell (s_{k,m}^\ell)^* \} - \sqrt{\Gamma^\ell \sigma_{\text{eff}}^2} \right), \quad \forall m, \ell, \end{aligned} \quad (23b)$$

$$\|\mathbf{W}_k^\ell \mathbf{s}^\ell\|_2^2 \leq \frac{p_{\text{tot}}}{L}, \quad \forall \ell, \quad (23c)$$

$$\|(\mathbf{I}_{N_r} - \mathbf{H}_i \mathbf{H}_i^\dagger) \mathbf{H}_k \mathbf{W}_k^\ell \mathbf{s}^\ell\|_2^2 \leq \epsilon, \quad \forall i \in \mathcal{A}, \forall \ell, \quad (23d)$$

$$\Gamma^\ell \geq \Gamma, \quad \forall \ell. \quad (23e)$$

where (23a) ensures the SDR constraints for communication reliability, (23b) enforces CI conditions at the symbol level, ensuring that the received signals lie within the constructive region of the modulation constellation, (23c) imposes the power budget for each symbol interval, where  $p_{\text{tot}}$  is the total transmit power, and (23d) incorporates the transmission anonymity constraint, determined in (14). We highlight that problem P0 implements a two-level fairness criterion, guaranteeing uniformly reliable transmission across both data streams  $\forall m$  and timeslots  $\forall \ell$ .

Since all constraints in (23a)–(23e) are imposed independently per timeslot, and the precoder  $\mathbf{W}_k^\ell$  appears only in constraints indexed by the same  $\ell$ , the problem P0 admits a per-timeslot decomposition. Accordingly, for a given timeslot  $\ell$ , we can solve the following subproblem (dropping the index  $\ell$  for notational simplicity):

$$\begin{aligned} \text{P1: } & \max_{\mathbf{W}_k, \Gamma} \Gamma \\ \text{s.t. } & \frac{\|\mathbf{c}_{k,m} \mathbf{H}_{k,m} \mathbf{W}_k \mathbf{s}\|^2}{|\mathcal{S}_m| \sigma_k^2} \geq \Gamma, \quad \forall m, \end{aligned} \quad (24a)$$

$$\begin{aligned} & |\Im \{ \mathbf{c}_{k,m} \mathbf{H}_{k,m} \mathbf{W}_k \mathbf{s} (s_{k,m})^* \}| \leq \tan \theta \\ & \times \left( \Re \{ \mathbf{c}_{k,m} \mathbf{H}_{k,m} \mathbf{W}_k \mathbf{s} (s_{k,m})^* \} - \sqrt{\Gamma \sigma_{\text{eff}}^2} \right), \quad \forall m, \end{aligned} \quad (24b)$$

$$\|\mathbf{W}_k \mathbf{s}\|_2^2 \leq \frac{p_{\text{tot}}}{L}, \quad (24c)$$

$$\|(\mathbf{I}_{N_r} - \mathbf{H}_i \mathbf{H}_i^\dagger) \mathbf{H}_k \mathbf{W}_k \mathbf{s}\|_2^2 \leq \epsilon, \quad \forall i \in \mathcal{A}. \quad (24d)$$

Let  $\Gamma_\ell^*$  denote the optimal value of problem P1 for timeslot  $\ell$ . The optimal solution to the original problem P0 is then expressed as

$$\Gamma^* = \min_{\ell \in \{1, \dots, L\}} \Gamma_\ell^*, \quad (25)$$

with  $\mathbf{W}_k^\ell$  selected as the optimizer of the corresponding per-timeslot problem.

Problem P1 is non-convex due to the SDR constraints (24a) and the CI constraints (24b). To obtain a tractable design, we adopt<sup>3</sup> a standard CI margin maximization approach [22]. Specifically, we define the (real) CI margin as

$$\gamma \triangleq \sqrt{\Gamma \sigma_{\text{eff}}^2}, \quad (26)$$

and directly maximize  $\gamma$ , which enforces a common lower bound on the in-phase constructive component for all streams. For QPSK,  $|s_{k,m}| = 1$ , and the CI constraint implies  $\Re\{u_m\} \geq \gamma$ , where  $u_m \triangleq \mathbf{c}_{k,m} \mathbf{H}_{k,m} \mathbf{W}_k \mathbf{s} (s_{k,m})^*$ . Therefore,  $|u_m| \geq \Re\{u_m\} \geq \gamma$ , which further yields  $\|\mathbf{c}_{k,m} \mathbf{H}_{k,m} \mathbf{W}_k \mathbf{s}\|^2 = |u_m|^2 \geq \gamma^2 = \Gamma |\mathcal{S}_m| \sigma_k^2$ ,  $\forall m$ , i.e., (24a) is implied by the CI constraints and can thus be omitted. Consequently, we equivalently solve

$$\begin{aligned} \text{P2: } & \max_{\mathbf{W}_k, \gamma} \gamma \\ \text{s.t. } & |\Im \{ \mathbf{c}_{k,m} \mathbf{H}_{k,m} \mathbf{W}_k \mathbf{s} (s_{k,m})^* \}| \leq \tan \theta \\ & (\Re \{ \mathbf{c}_{k,m} \mathbf{H}_{k,m} \mathbf{W}_k \mathbf{s} (s_{k,m})^* \} - \gamma), \quad \forall m, \end{aligned} \quad (27a)$$

$$\|\mathbf{W}_k \mathbf{s}\|_2^2 \leq \frac{p_{\text{tot}}}{L}, \quad (27b)$$

$$\|(\mathbf{I}_{N_r} - \mathbf{H}_i \mathbf{H}_i^\dagger) \mathbf{H}_k \mathbf{W}_k \mathbf{s}\|_2^2 \leq \epsilon, \quad \forall i \in \mathcal{A}. \quad (27c)$$

We highlight that problem P2 is convex second-order cone programming (SOCP), due to an affine objective function with linear and second-order cone (SOC) constraints [40].

<sup>3</sup>Although problem P1 can be tackled via successive convex approximation (SCA) [40], [41] by iteratively convexifying the nonconvex SDR constraints, such approaches typically converge only to a stationary point with initialization-dependent solution and require an additional bisection/inner-loop procedure to handle  $\sqrt{\Gamma}$  in the CI constraints. In contrast, the CI-margin reformulation in P2 admits an SOCP representation and can be solved globally; hence, we adopt P2 as a tractable surrogate for P1.

The CI constraint in (27a) is linear, since the absolute-value inequality can be rewritten as two affine inequalities. The power constraint in (27b) and the anonymity constraint in (27c) are SOC constraints of the form  $\|\mathbf{A}x\|_2 \leq b$ . Hence, P2 can be efficiently solved by any convex optimization tool. Algorithm 1 summarizes our proposed anonymous precoding design.

### E. Complexity Analysis

The per-timeslot problem (27) is SOCP and can be solved using a primal–dual interior-point method (IPM). The worst-case complexity of conic programs with SOC and linear matrix inequality (LMI) constraints using a standard IPM scales as [22], [42]

$$\mathcal{C} = \mathcal{O}\left(\ln\frac{1}{\tau} \sqrt{\beta} (C_{\text{form}} + C_{\text{fact}})\right), \quad (28)$$

where  $\tau > 0$  denotes the target accuracy and  $\beta$  is the barrier parameter, given by

$$\beta = \sum_{j=1}^p q_j + 2v, \quad (29)$$

with  $p$  denoting the number of LMI constraints of sizes  $\{q_j\}_{j=1}^p$ , and  $v$  denoting the number of SOC constraints. The per-iteration computational costs for forming and factorizing the Newton system are upper bounded by [42]

$$\begin{aligned} C_{\text{form}} &= n_{\text{var}} \sum_{j=1}^p q_j^3 + n_{\text{var}}^2 \sum_{j=1}^p q_j^2 + n_{\text{var}} \sum_{j=1}^v u_j^2, \\ C_{\text{fact}} &= n_{\text{var}}^3, \end{aligned} \quad (30)$$

where  $n_{\text{var}}$  is the number of decision variables and  $u_j$  is the dimension of the  $j^{\text{th}}$  SOC constraint.

For problem P2, constraint (27a) is equivalent to two affine inequalities per data stream, yielding  $2N_s$  scalar linear constraints. These can be treated as  $2N_s$  size-one LMIs, i.e.,  $p = 2N_s$  and  $q_j = 1$ . Constraint (27b) contributes one SOC constraint of size  $N_t$ , and constraint (27c) contributes  $|\mathcal{A}| = a$  SOC constraints of size  $N_r$ . Hence,  $v = 1 + a$  and  $\beta = 2N_s + 2(1 + a)$ . In addition, since  $\mathbf{W}_k \in \mathbb{C}^{N_t \times N_s}$  and  $\gamma \in \mathbb{R}$ , the real-valued problem has  $n_{\text{var}} = 2N_t N_s + 1$  decision variables. Substituting these quantities yields the worst-case complexity of solving P2 per timeslot as

$$\begin{aligned} \mathcal{C}_{\text{P2}} &= \mathcal{O}\left(\ln\frac{1}{\tau} \sqrt{2N_s + 2(1 + a)} \right. \\ &\quad \left. \times [2N_s n_{\text{var}}^2 + n_{\text{var}}(2N_s + N_t^2 + aN_r^2) + n_{\text{var}}^3] \right). \end{aligned} \quad (31)$$

Since the precoder is designed independently across  $L$  timeslots, the overall algorithm complexity scales linearly with  $L$ . Moreover, since the Newton-system factorization term  $n_{\text{var}}^3$  is dominant in typical MIMO regimes, the total complexity can be approximated as

$$\mathcal{C}_{\text{total}} \approx \mathcal{O}\left(L \ln\frac{1}{\tau} \sqrt{2N_s + 2(1 + a)} (N_t N_s)^3\right). \quad (32)$$

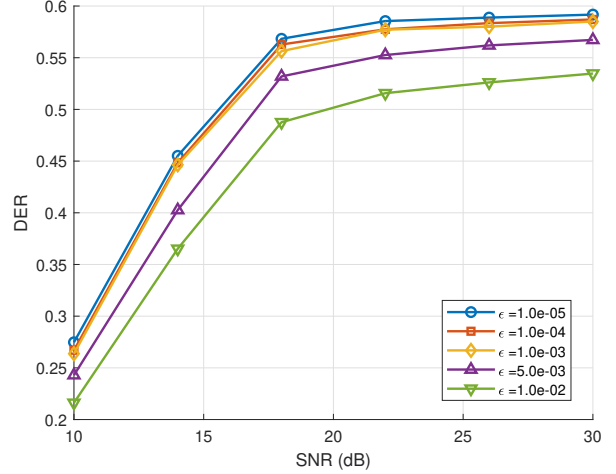


Fig. 2. DER vs. SNR under different anonymity relaxations  $\epsilon$ .

## V. SIMULATION RESULTS

In this section, we present simulation results to evaluate the detection performance and anonymity behavior of the proposed framework. In each Monte Carlo trial, the index of the active user  $k$  is randomly selected from all  $K$  candidates to ensure statistical fairness. The alias user is then randomly chosen from the remaining  $K - 1$  candidates to form an alias set with size  $a = 1$ . Unless otherwise specified, the following parameters are used throughout the simulations: The total number of users is  $K = 15$ , the number of receive antennas is  $N_r = 12$ , the number of transmit antennas is  $N_t = 8$ , the number of data streams is  $N_s = 4$ , and the block length is  $L = 30$ . In addition, the noise variance at any non-transmitting user  $i \neq k$  is modeled as a random perturbation around that of the true transmitter, given by

$$\sigma_i^2 = 10^{\beta_i/10} \sigma_k^2, \quad \forall i \neq k, \quad (33)$$

where  $\{\beta_i\}$  are i.i.d. random variables uniformly distributed over  $[-d, d]$ , i.e.,  $\beta_i \sim \mathcal{U}[-d, d]$ , representing the relative deviation of each user's noise variance from that of the true transmitter, and  $d$  denotes the half-range of noise variation in the logarithmic domain. We set  $d = 1.5$  dB, which introduces moderate randomness yet controlled heterogeneity in the noise levels. Finally, we clarify that all SNRs in this section are defined as transmit SNRs.

In this section, we do not provide performance comparison with existing precoders, as conventional precoder designs (e.g., SVD/MMSE) provide near-zero anonymity in the considered SNR range. Meanwhile, recently proposed physical-layer anonymous precoders [22]–[24] rely on fundamentally different system assumptions and formulations (e.g., full-multiplexing without combiners, full-diversity single-stream transmission, or homogeneous-noise closed-form DER analysis). Adapting them to our heterogeneous-noise multiplexing–diversity framework would substantially alter their structure and lead to unfair or impractical comparisons.

Fig. 2 shows the DER performance as a function of the SNR for different anonymity constraint relaxation parameters

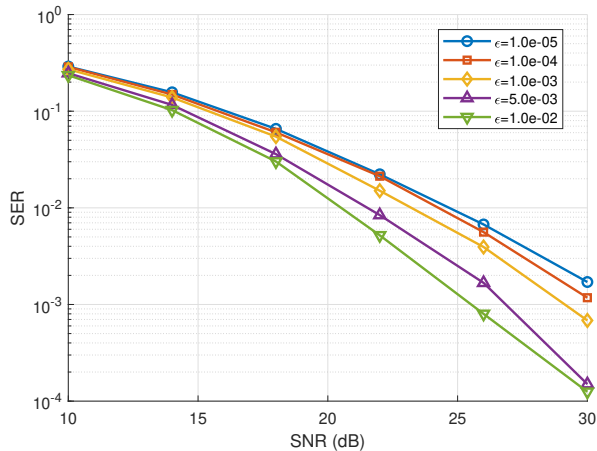


Fig. 3. Average symbol error rate (SER) vs. SNR with different  $\epsilon$ .

$\epsilon$ . Interestingly, the DER increases with the SNR, indicating that higher transmit power enhances anonymity. This behavior can be explained by examining the expected difference expression  $E[D_i]$  in Lemma 1. Specifically, the noise-variance-related constant term remains essentially independent of the SNR, whereas the signal-dependent trace-difference term grows proportionally with the signal power. Since the proposed anonymous precoder explicitly constrains this signal-dependent component, its relative influence on the test statistic becomes more pronounced at high SNRs, i.e., degrading the receiver's identification capability and increasing the DER. Moreover, smaller  $\epsilon$  generally imposes tighter anonymity constraints and consistently yields higher DER. However, when  $\epsilon$  becomes sufficiently small (e.g., below  $10^{-3}$ ), the curves exhibit saturation, suggesting that further tightening provides negligible additional anonymity improvement.

Fig. 3 illustrates the SER performance of the considered system against the SNR for different anonymity relaxations. As expected, increasing the SNR improves communication reliability for all cases, resulting in a monotonic SER reduction. In particular, for relatively high SNRs, the SER drops to below  $10^{-3}$ , which is a commonly accepted reliability threshold in communication systems. Moreover, comparing curves with different  $\epsilon$  values reveals that looser anonymity constraints (larger  $\epsilon$ ) achieve lower SER, since the anonymity precoder has greater freedom to optimize signal alignment for detection. Conversely, tighter anonymity enforcement restricts the feasible precoding space and slightly degrades reliability. These results clearly demonstrate the inherent tradeoff between anonymity and communication performance. In addition, when the anonymity constraint becomes sufficiently tight (e.g.,  $10^{-5}$  or even  $10^{-4}$ ), further reduction in  $\epsilon$  brings negligible changes to the overall performance, indicating that reliability degradation also exhibits a saturation effect similar to results in Fig. 2.

Fig. 4 illustrates the SER-DER relationship across different transmit SNRs, where each point on the curves corresponds to a different anonymity relaxation parameter  $\epsilon$ . As  $\epsilon$  decreases, i.e., the anonymity constraint becomes tighter (higher DER), the SER increases, implying degraded communication reliability.

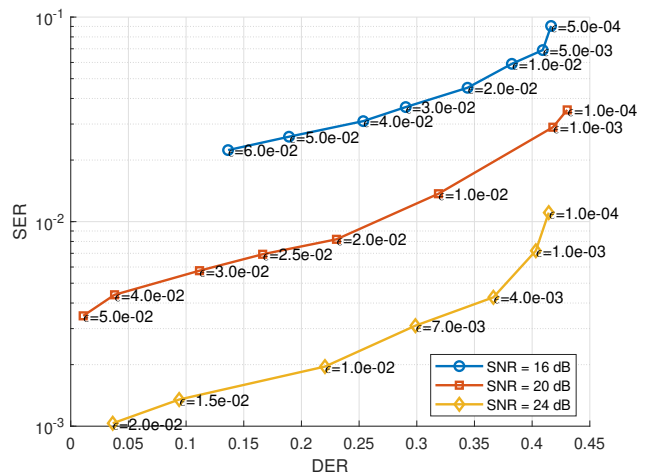


Fig. 4. SER-DER tradeoff under different transmit SNRs and  $\epsilon$ .

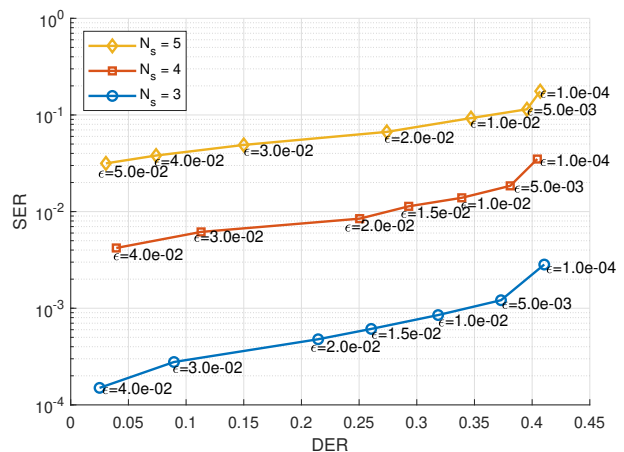


Fig. 5. SER-DER tradeoff under different number of data streams  $N_s$  and  $\epsilon$ . The SNR is set to 20 dB.

ability. This SER-DER relationship explicitly demonstrates the cost of anonymity in terms of detection reliability. For all SNR levels, the curves display a consistent monotonic tradeoff pattern between anonymity and reliability. As an illustration at a fixed anonymity level (DER  $\approx 0.3$ ), increasing the SNR from 16 dB to 24 dB reduces the SER from  $3.6 \times 10^{-2}$  to  $3.1 \times 10^{-3}$ , corresponding to nearly one order-of-magnitude improvement in reliability. Nevertheless, at higher SNRs, the suitable values of  $\epsilon$  become smaller, indicating that the system becomes more sensitive to  $\epsilon$ . In particular, when  $\epsilon$  becomes very small (e.g., below  $10^{-3}$ ), the SER increases sharply while DER improves only marginally, indicating diminishing anonymity returns. This also suggests that loosening anonymity requirements leads to significant reliability improvement in the tight  $\epsilon$  region.

Fig. 5 investigates the impact of the number of transmitted data streams  $N_s$  on the anonymity-reliability tradeoff, where the SNR is fixed at 20 dB. We see that increasing  $N_s$  enhances anonymity but degrades communication reliability in terms of the SER. While all three curves follow the same overall

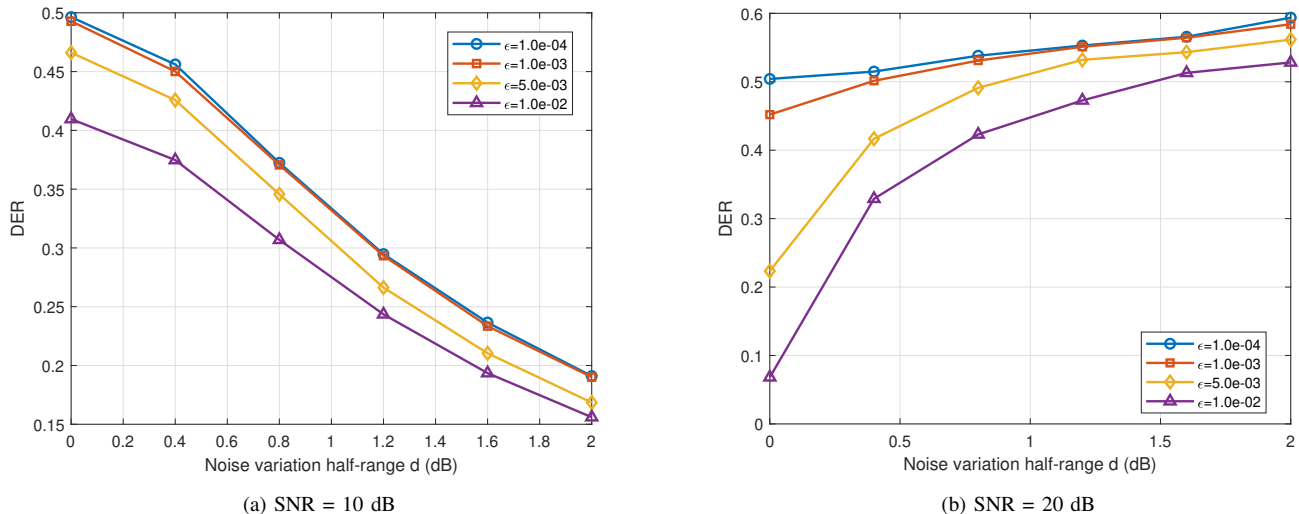


Fig. 6. DER versus the noise-variation half-range parameter  $d$  under different anonymity relaxation parameter  $\epsilon$ .

tradeoff pattern, the curve with low data stream (e.g.,  $N_s = 3$ ) exhibits a larger DER variation over the same range of  $\epsilon$ , and its slope is steeper compared with the cases with higher  $N_s$ . This indicates that the configurations with fewer data streams are more sensitive to changes in the anonymity constraint  $\epsilon$ , and achieving the same level of DER improvement requires a relatively larger increase in the SER. Consequently, aggressive anonymity enforcement can lead to rapid reliability degradation in low-stream configurations.

In Fig. 6, we investigate how the heterogeneity of user-dependent noise levels affects the system's anonymity performance. To this end, we plot the DER as a function of the log-domain noise-variation half-range parameter  $d$ . At the low SNR (Fig. 6(a), 10 dB), the DER decreases as  $d$  increases, indicating reduced anonymity. In this regime, transmitter identification is primarily determined by noise statistics, and larger dispersion in user noise variances makes the competing hypotheses more distinguishable, which enables more reliable detection. In contrast, at the high SNR (Fig. 6(b), 20 dB), the trend reverses and the DER increases with  $d$ . Here, the signal-dependent trace term controlled by the anonymous precoder dominates the likelihood metric, while the relative contribution of the noise-dependent constant becomes secondary. Larger alias noise variances reduce the normalized trace difference between hypotheses, which decreases hypothesis separability and consequently improves anonymity. These results demonstrate that the effect of hardware-induced noise heterogeneity on transmitter identification is strongly dependent on the operating SNR.

Fig. 7 shows the noise-dependent constant term as a function of the noise-variance ratio  $r$ . The curve is non-monotonic and concave, intersecting zero at  $r = 1$  and at a second point  $r_- < 1$ . Consequently, the constant term is positive only within the narrow interval  $r_- < r < 1$ , namely, when the alias user has a slightly smaller noise variance than the true user. Only in this region can the alias hypothesis produce a larger likelihood value and meaningfully degrade transmitter identification. For larger deviations in either direction, the constant

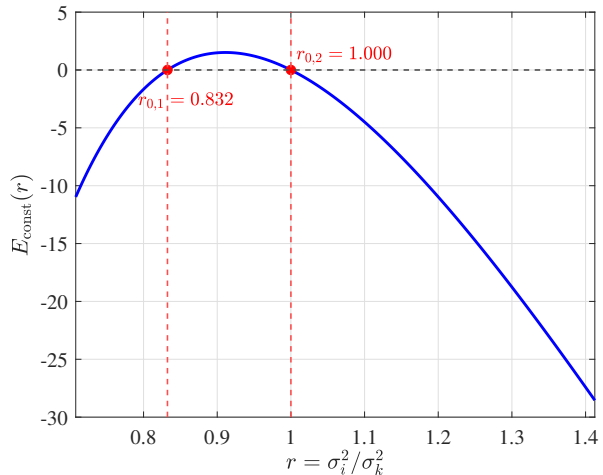


Fig. 7. Noise-dependent constant term  $E_{\text{const}}$  vs. the noise-variance ratio  $r = \sigma_i^2 / \sigma_k^2$ .

term becomes negative, which increases hypothesis separability and facilitates detection. We clarify that this behavior highlights the effect of noise heterogeneity on anonymity. When noise statistics dominate, greater variance disparity makes users more distinguishable and reduces DER. In contrast, when the signal-dependent component dominates, larger alias noise variances attenuate the normalized trace difference and reduce separability, resulting in improved anonymity. Thus, the influence of noise heterogeneity on the DER depends on which term governs the test statistic.

## VI. CONCLUSION

We studied physical-layer transmitter anonymity in uplink multi-antenna systems, where we considered a symbol-aware receiver performing multi-hypothesis transmitter identification using the known symbol matrix, CSI, and transmitter-dependent hardware noise statistics. To enable tractable design, we introduced a KLD-based metric to quantify pairwise

anonymity between the active and alias users and derived the corresponding anonymity constraint. We further proposed the P-EGC to enhance communication reliability at the receiver and developed the corresponding anonymous precoding scheme under spatial multiplexing. The overall design was formulated as a convex optimization problem. Simulation results, measured in terms of the DER and SER, showed that the proposed scheme significantly improves transmitter anonymity compared with anonymity-unaware precoding schemes while maintaining reliable communication performance.

#### APPENDIX A PROOF OF LEMMA 1

This appendix derives the KLD between the distributions of the received signal  $\mathbf{Y}$  under the true hypothesis  $p_k$  and a false hypothesis  $p_i$ , as follows:

From (6), each test statistic consists of a linear combination of a constant term and a random term involving the Frobenius norm. Hence, we define

$$F_k = \|\widehat{\mathbf{Y}}_k - \mathbf{Y}\|_F^2 \text{ and } F_i = \|\widehat{\mathbf{Y}}_i - \mathbf{Y}\|_F^2. \quad (\text{A.1})$$

Substituting the reconstructed signals (3) and (4) into (A.1) yields

$$\begin{aligned} F_k &= \left\| \mathbf{H}_k \mathbf{H}_k^\dagger \mathbf{N}_k \mathbf{S}^\dagger \mathbf{S} - \mathbf{N}_k \right\|_F^2, \\ F_i &= \left\| \mathbf{H}_i \mathbf{H}_i^\dagger \mathbf{Y} \mathbf{S}^\dagger \mathbf{S} - \mathbf{Y} \right\|_F^2. \end{aligned} \quad (\text{A.2})$$

We first compute the expectations of  $F_k$  and  $F_i$ . Using the properties of the Frobenius norm and that  $\mathbf{N}_k$  is zero-mean CSCG noise with covariance  $\sigma_k^2 \mathbf{I}_{N_r L}$ , the expectation of  $F_k$  is given by

$$\begin{aligned} \mathbb{E}[F_k] &= \mathbb{E} \left[ \left\| \mathbf{H}_k \mathbf{H}_k^\dagger \mathbf{N}_k \mathbf{S}^\dagger \mathbf{S} - \mathbf{N}_k \right\|_F^2 \right] \\ &= \mathbb{E} \left[ \text{tr} \left( (\mathbf{H}_k \mathbf{H}_k^\dagger \mathbf{N}_k \mathbf{S}^\dagger \mathbf{S} - \mathbf{N}_k)^H (\mathbf{H}_k \mathbf{H}_k^\dagger \mathbf{N}_k \mathbf{S}^\dagger \mathbf{S} - \mathbf{N}_k) \right) \right] \\ &= \text{tr} \left( \mathbb{E}[\mathbf{N}_k^H \mathbf{N}_k] \right) - \text{tr} \left( \mathbb{E}[\mathbf{N}_k \mathbf{S}^\dagger \mathbf{S} \mathbf{N}_k^H] \mathbf{H}_k \mathbf{H}_k^\dagger \right) \\ &= \sigma_k^2 N_r L - \sigma_k^2 N_t N_s. \end{aligned} \quad (\text{A.3})$$

Similarly, the expectation of  $F_i$  is obtained as

$$\begin{aligned} \mathbb{E}[F_i] &= \mathbb{E} \left[ \left\| \mathbf{H}_i \mathbf{H}_i^\dagger \mathbf{Y} \mathbf{S}^\dagger \mathbf{S} - \mathbf{Y} \right\|_F^2 \right] \\ &= \mathbb{E} \left[ \text{tr} \left( (\mathbf{H}_i \mathbf{H}_i^\dagger \mathbf{Y} \mathbf{S}^\dagger \mathbf{S} - \mathbf{Y})^H (\mathbf{H}_i \mathbf{H}_i^\dagger \mathbf{Y} \mathbf{S}^\dagger \mathbf{S} - \mathbf{Y}) \right) \right] \\ &= \text{tr} \left( \mathbb{E}[\mathbf{Y}^H \mathbf{Y}] \right) - \text{tr} \left( \mathbb{E}[\mathbf{Y}^H \mathbf{H}_i \mathbf{H}_i^\dagger \mathbf{Y}] \mathbf{S}^\dagger \mathbf{S} \right) \\ &= \sigma_k^2 N_r L - \sigma_k^2 N_t N_s + \text{tr} \left( \mathbf{S}^H \mathbf{W}_k^H \mathbf{H}_k^H \mathbf{H}_k \mathbf{W}_k \mathbf{S} \right) \\ &\quad - \text{tr} \left( \mathbf{S}^H \mathbf{W}_k^H \mathbf{H}_k^H \mathbf{H}_i \mathbf{H}_i^\dagger \mathbf{H}_k \mathbf{W}_k \mathbf{S} \right). \end{aligned} \quad (\text{A.4})$$

Consequently, the corresponding expectations of test statistics  $T_k$  and  $T_i$  follow directly by linearity of expectation as

$$\begin{aligned} \mathbb{E}[T_k] &= -N_r L \ln(\pi \sigma_k^2) - (N_r L - N_s N_t), \\ \mathbb{E}[T_i] &= -N_r L \ln(\pi \sigma_i^2) - \frac{\sigma_k^2}{\sigma_i^2} (N_r L - N_s N_t) \\ &\quad - \frac{1}{\sigma_i^2} \left( \text{tr} \left( \mathbf{S}^H \mathbf{W}_k^H \mathbf{H}_k^H \mathbf{H}_k \mathbf{W}_k \mathbf{S} \right) \right. \\ &\quad \left. - \text{tr} \left( \mathbf{S}^H \mathbf{W}_k^H \mathbf{H}_k^H \mathbf{H}_i \mathbf{H}_i^\dagger \mathbf{H}_k \mathbf{W}_k \mathbf{S} \right) \right). \end{aligned} \quad (\text{A.5})$$

We next define

$$p_k(\mathbf{Y}) \triangleq p(\mathbf{Y}; \widehat{\mathbf{W}}_k, \mathcal{H}_k) \text{ and } p_i(\mathbf{Y}) \triangleq p(\mathbf{Y}; \widehat{\mathbf{W}}_i, \mathcal{H}_i),$$

such that  $T_k = \ln p_k(\mathbf{Y})$  and  $T_i = \ln p_i(\mathbf{Y})$ . When hypothesis  $\mathcal{H}_k$  is true,  $\mathbf{Y} \sim p_k(\mathbf{Y})$ , and thus

$$\begin{aligned} \mathbb{E}[T_k] &= \int p_k(\mathbf{Y}) \ln p_k(\mathbf{Y}) d\mathbf{Y}, \\ \mathbb{E}[T_i] &= \int p_k(\mathbf{Y}) \ln p_i(\mathbf{Y}) d\mathbf{Y}. \end{aligned} \quad (\text{A.6})$$

Taking their difference yields

$$\begin{aligned} \mathbb{E}[T_i] - \mathbb{E}[T_k] &= \int p_k(\mathbf{Y}) \left( \ln p_i(\mathbf{Y}) - \ln p_k(\mathbf{Y}) \right) d\mathbf{Y} \\ &= - \int p_k(\mathbf{Y}) \ln \frac{p_k(\mathbf{Y})}{p_i(\mathbf{Y})} d\mathbf{Y} \\ &= -D_{\text{KL}}(p_k \| p_i), \end{aligned} \quad (\text{A.7})$$

which implies that the KLD between  $p_k$  and  $p_i$  can be computed directly from the difference between the expectations of  $T_i$  and  $T_k$ , without requiring the full distributions of  $T_k$  and  $T_i$ . Finally, substituting (A.5) into (A.7) establishes the result in Lemma 1. ■

#### REFERENCES

- [1] D. C. Nguyen *et al.*, "6G Internet of Things: A comprehensive survey," *IEEE Internet Things J.*, vol. 9, no. 1, pp. 359–383, Jun. 2022.
- [2] K. B. Letaief, W. Chen, Y. Shi, J. Zhang, and Y.-J. A. Zhang, "The roadmap to 6G: AI empowered wireless networks," *IEEE Commun. Mag.*, vol. 57, no. 8, pp. 84–90, Aug. 2019.
- [3] W. Saad, M. Bennis, and M. Chen, "A vision of 6G wireless systems: Applications, trends, technologies, and open research problems," *IEEE Netw.*, vol. 34, no. 3, pp. 134–142, May/June 2020.
- [4] M. Mitev, A. Chorti, H. V. Poor, and G. P. Fettweis, "What physical layer security can do for 6G security," *IEEE Open J. Veh. Technol.*, vol. 4, pp. 375–388, 2023.
- [5] V.-L. Nguyen, P.-C. Lin, B.-C. Cheng, R.-H. Hwang, and Y.-D. Lin, "Security and privacy for 6G: A survey on prospective technologies and challenges," *IEEE Commun. Surveys Tuts.*, vol. 23, no. 4, pp. 2384–2428, 4th Quart., 2021.
- [6] G. Tripi, A. Iacobelli, L. Rinieri, and M. Prandini, "Security and trust in the 6G era: Risks and mitigations," *Electronics*, vol. 13, no. 11, p. 2162, 2024.
- [7] Y. Yang, L. Wu, G. Yin, L. Li, and H. Zhao, "A survey on security and privacy issues in Internet-of-Things," *IEEE Internet Things J.*, vol. 4, no. 5, pp. 1250–1258, Oct. 2017.
- [8] C. Sandeepa, B. Siniarski, N. Kourtellis, S. Wang, and M. Liyanage, "A survey on privacy for B5G/6G: New privacy challenges, and research directions," *J. Ind. Inf. Integr.*, vol. 30, p. 100405, Nov. 2022.
- [9] P. Angueira *et al.*, "A survey of physical layer techniques for secure wireless communications in industry," *IEEE Commun. Surveys Tuts.*, vol. 24, no. 2, pp. 810–838, 2nd Quart., 2022.
- [10] M. Bloch and J. Barros, *Physical-Layer Security: From Information Theory to Security Engineering*. Cambridge, UK: Cambridge University Press, 2011.

- [11] X. Zhou, L. Song, and Y. Zhang, *Physical Layer Security in Wireless Communications*. Boca Raton, FL, USA: CRC Press, 2016.
- [12] M. T. Mamaghani, X. Zhou, N. Yang, A. L. Swindlehurst, and H. V. Poor, "Performance analysis of finite blocklength transmissions over wiretap fading channels: An average information leakage perspective," *IEEE Trans. Wirel. Commun.*, vol. 23, no. 10, pp. 13 252–13 266, Oct. 2024.
- [13] Z. Wei, P. Wang, A. P. Petropulu, C. Masouros, and S. Sun, "Physical layer anonymous communications in trustworthy 6G: Fundamentals, recent advances, and future trends," *IEEE Wireless Commun.*, vol. 32, no. 2, pp. 26–32, Apr. 2025.
- [14] B. A. Bash, D. Goeckel, D. Towsley, and S. Guha, "Hiding information in noise: Fundamental limits of covert wireless communication," *IEEE Commun. Mag.*, vol. 53, no. 12, pp. 26–31, Dec. 2015.
- [15] S.-F. Tzeng, S.-J. Hwang, T. Li, X. Wang, P.-H. Huang, and M. K. Khan, "Enhancing security and privacy for identity-based batch verification scheme in VANETs," *IEEE Trans. Veh. Technol.*, vol. 66, no. 4, pp. 3235–3248, Apr. 2017.
- [16] Z. Lu, G. Qu, and Z. Liu, "A survey on recent advances in vehicular network security, trust, and privacy," *IEEE Trans. Intell. Transp. Syst.*, vol. 20, no. 2, pp. 760–776, Feb. 2019.
- [17] P. Tedeschi, F. A. Al Nuaimi, A. I. Awad, and E. Natalizio, "Privacy-aware remote identification for unmanned aerial vehicles: Current solutions, potential threats, and future directions," *IEEE Trans. Ind. Informat.*, vol. 20, no. 2, pp. 1069–1080, Feb. 2024.
- [18] A. Fotouhi *et al.*, "Survey on UAV cellular communications: Practical aspects, standardization advancements, regulation, and security challenges," *IEEE Commun. Surveys Tuts.*, vol. 21, no. 4, pp. 3417–3442, 4th Quart., 2019.
- [19] S. Pai *et al.*, "Confidentiality in sensor networks: Transactional information," *IEEE Secur. Privacy Mag.*, vol. 6, no. 4, pp. 28–35, Jul./Aug. 2008.
- [20] P. Gope and T. Hwang, "BSN-Care: A secure IoT-based modern healthcare system using body sensor network," *IEEE Sensors J.*, vol. 16, no. 5, pp. 1368–1376, Mar. 2016.
- [21] Z. Wei, C. Masouros, H. V. Poor, A. P. Petropulu, and L. Hanzo, "Physical layer anonymous precoding: The path to privacy-preserving communications," *IEEE Wireless Commun.*, vol. 29, no. 2, pp. 154–160, Apr. 2022.
- [22] Z. Wei, F. Liu, C. Masouros, and H. V. Poor, "Fundamentals of physical layer anonymous communications: Sender detection and anonymous precoding," *IEEE Trans. Wirel. Commun.*, vol. 21, no. 1, pp. 64–79, Jan. 2022.
- [23] Z. Wei, C. Masouros, P. Wang, X. Zhu, J. Wang, and A. P. Petropulu, "Physical layer anonymous precoding design: From the perspective of anonymity entropy," *IEEE J. Sel. Areas Commun.*, vol. 40, no. 11, pp. 3224–3238, Nov. 2022.
- [24] Z. Wei, C. Masouros, X. Zhu, P. Wang, and A. P. Petropulu, "PHY layer anonymous precoding: Sender detection performance and diversity-multiplexing tradeoff," *IEEE Trans. Wirel. Commun.*, vol. 23, no. 5, pp. 4531–4545, May 2024.
- [25] Y. Cui, Z. Wei, S. Sun, X. Zhu, C. Masouros, and A. P. Petropulu, "Physical layer anonymous precoding under CSI and hardware-imperfections: A KLD-based approach," *IEEE Trans. Wireless Commun.*, vol. 25, pp. 6225–6239, 2025.
- [26] Y. Cui, Z. Wei, C. Masouros, X. Zhu, and H. Tang, "On the closed-form detection error rate analysis in physical layer anonymous communications," *IEEE Trans. Veh. Technol.*, vol. 73, no. 8, pp. 12 195–12 200, Aug. 2024.
- [27] M. Wang, Z. Wei, C. Masouros, A. Guo, and N. Jia, "Closed-form detection error rate analysis in PHY-anonymous MIMO MAC channel," *IEEE Trans. Veh. Technol.*, 2025, early Access.
- [28] R. Song and H. Tang, "LAA: Link-layer anonymous access for tactical MANETs," in *Proc. IEEE Military Communications Conf. (MILCOM)*, Orlando, FL, USA, 2012, pp. 1–7.
- [29] C. Studer, M. Wenk, and A. Burg, "MIMO transmission with residual transmit-RF impairments," in *Proc. Int. ITG Workshop Smart Antennas (WSA)*, Bremen, Germany, 2010, pp. 189–196.
- [30] E. Björnson, J. Hoydis, M. Kountouris, and M. Debbah, "Hardware impairments in large-scale MISO systems: Energy efficiency, estimation, and capacity limits," in *Proc. 18th Int. Conf. Digit. Signal Process (DSP)*, Santorini, Greece, 2013, pp. 1–6.
- [31] X. Zhang, M. Matthaiou, E. Björnson, M. Coldrey, and M. Debbah, "On the MIMO capacity with residual transceiver hardware impairments," in *Proc. IEEE Int. Conf. Commun. (ICC)*, Sydney, Australia, 2014, pp. 5299–5305.
- [32] H. Suzuki, T. V. A. Tran, I. B. Collings, G. Daniels, and M. Hedley, "Transmitter noise effect on the performance of a MIMO-OFDM hardware implementation achieving improved coverage," *IEEE J. Sel. Areas Commun.*, vol. 26, no. 6, pp. 867–876, Aug. 2008.
- [33] S. M. Kay, *Fundamentals of Statistical Signal Processing, Volume 2: Detection Theory*. Prentice Hall, 1998.
- [34] T. M. Cover and J. A. Thomas, *Elements of Information Theory*. John Wiley & Sons, 1999.
- [35] C. Masouros and G. Zheng, "Exploiting known interference as green signal power for downlink beamforming optimization," *IEEE Trans. Signal Process.*, vol. 63, no. 14, pp. 3628–3640, Jul. 2015.
- [36] Z. Wei, C. Masouros, K.-K. Wong, and X. Kang, "Multi-cell interference exploitation: Enhancing the power efficiency in cell coordination," *IEEE Trans. Wireless Commun.*, vol. 19, no. 1, pp. 547–562, Jan. 2020.
- [37] Z. Wei, C. Masouros, and F. Liu, "Secure directional modulation with few-bit phase shifters: Optimal and iterative-closed-form designs," *IEEE Trans. Commun.*, vol. 69, no. 1, pp. 486–500, Jan. 2021.
- [38] A. Li, C. Masouros, B. Vucetic, Y. Li, and A. L. Swindlehurst, "Interference exploitation precoding for multi-level modulations: Closed-form solutions," *IEEE Trans. Commun.*, vol. 69, no. 1, pp. 291–308, Jan. 2021.
- [39] Z. Wei, J. Wang, C. Masouros, T. Xu, J. Chen, and A. Li, "Sub-block level interference exploitation precoding in satellite communications," in *Proc. Int. Wireless Commun. Mobile Comput. Conf. (IWCMC)*, Limassol, Cyprus, 2024, pp. 0537–0542.
- [40] S. Boyd and L. Vandenberghe, *Convex Optimization*. Cambridge, U.K.: Cambridge Univ. Press, 2004.
- [41] M. T. Mamaghani and Y. Hong, "Aerial intelligent reflecting surface-enabled terahertz covert communications in beyond-5G Internet of Things," *IEEE Internet Things J.*, vol. 9, no. 19, pp. 19 012–19 033, Oct. 2022.
- [42] K.-Y. Wang, A. M.-C. So, T.-H. Chang, W.-K. Ma, and C.-Y. Chi, "Outage constrained robust transmit optimization for multiuser MISO downlinks: Tractable approximations by conic optimization," *IEEE Trans. Signal Process.*, vol. 62, no. 21, pp. 5690–5705, Nov. 2014.